Investigation of Spatial Repeatability Using a Tire Force Measuring Mat

A. C. COLLOP, T. E. C. POTTER, D. CEBON, AND D. J. COLE

A portable mat for measuring the dynamic tire forces of commercial vehicles is described. The mat is 56 m long and 13 mm thick and has 141 capacitative strip sensors spaced at 0.4-m intervals. The accuracy of the mat for measuring dynamic tire forces generated by heavy commercial vehicles is assessed using an instrumented vehicle. The spatial repeatability of dynamic wheel loads generated by 14 uninstrumented articulated vehicles is investigated, and it is concluded that approximately half of the vehicles tested are likely to contribute to a repeatable pattern of road loading.

Dynamic tire forces are caused by vibration of a moving vehicle excited by road surface roughness. They are thought to be a significant cause of road damage, although the mechanisms are not well understood. Dynamic tire forces are influenced by vehicle speed, road roughness, and the design of the vehicle, particularly its suspension system.

There have been two main approaches to estimating the road-damaging effects of dynamic tire forces. Some researchers believe that the loading at each point along the road is essentially random, so that each point incurs forces statistically similar to each other point, and damage is uniformly distributed along the road. Studies in which such loading is assumed predict an increase in road damage of approximately 20 to 30 percent from dynamic loads (*1–3*). Other researchers believe that the peak forces applied by the heavy-vehicle fleet are concentrated at specific locations along the road (*4–6*), and thus some locations along the road may incur up to four times more damage than the average (*4*). This effect has been termed "spatial repeatability." The life of the road is then expected to be governed by damage at these heavily loaded areas.

Several studies indicate that a vehicle traveling over a road section at one speed generates a spatial distribution of dynamic loading that is repeated closely on subsequent test runs at the same speed (*4–9*). Hahn (*6*) suggests that because a large proportion of heavy vehicles tend to have similar geometry and dynamic characteristics and tend to travel at similar speeds, spatial repeatability of road loading may be expected in normal traffic flow. Vehicles in a particular class tend to have similar mass distributions and geometry because of the nature of vehicle construction and use regulations. There is, however, significant variation in suspension characteristics, although leaf-spring suspensions are fitted to the majority of heavy articulated vehicles (*10*).

Using a validated vehicle simulation, Cole and Cebon (*11,12*) examine the spatial repeatability of dynamic tire forces generated by a fleet of dynamically similar vehicles. They conclude that approximately two-thirds of the four-axle leaf-sprung articulated vehicles may contribute to a repeated pattern of road loading. Gyenes and Mitchell (*9*) sum the dynamic wheel loads generated by a variety of instrumented axles at particular locations on a test track in the United Kingdom. They observe that the sum of the wheel loads varied significantly more than would have been expected if the high loads had been distributed randomly over the track. Gyenes and Mitchell also performed a limited study of spatial repeatability using eight weigh-in-motion sensors mounted in a highway at 2.7-m spacings. Their preliminary results indicate some evidence of load concentration effects.

Substantial reductions in road damage could be achieved through regulating dynamic tire forces, if they are repeatable for normal traffic conditions. Research is therefore needed to establish whether loading patterns are random or repeatable for normal variations in the dynamic characteristics of heavy commercial vehicles.

MAT TESTS

Mat Installation

The research described in this paper was performed with a load measuring mat, developed by the authors in conjunction with Golden River Traffic Limited, for measuring the dynamic tire forces generated by heavy commercial vehicles (*13*). The mat contains capacitative strip sensors encapsulated in polyurethane tiles as shown schematically in Figure 1. The tiles are 1.2 m by 1.2 m by 13 mm thick, and each one contains three sensors (1.2-m long) laid transverse to the wheel path, 0.4 m apart.

Tests described in this paper were performed on the Transport Research Laboratory (TRL) test track during the winter months of 1991 and 1992. The mat was installed by TRL personnel on a long, straight section of the track. Each mat tile was attached to the brushed concrete surface by an adhesive sheet and six screws. There were 47 tiles in total, together containing 141 sensors, for an overall instrumented length of 56.4 m. Sheets of plywood were used to provide a ramp up to the mat and a run-off section, both

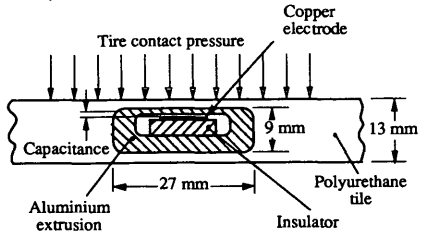

FIGURE 1 Cross section of capacitive strip sensor cast into polyurethane tile.

Engineering Department, Cambridge University, Cambridge CB2 1P2, England.

15 m long. The mat system was used in an earlier study for the Strategic Highway Research Program (SHRP) (*14,15*). The mat used in the present study incorporated the 32 tiles manufactured for the earlier U.S. SHRP study, as well as 15 new tiles.

Outputs of the sensors were logged and processed by nine Golden River Marksman M600 data-loggers. The data stored by each logger were transferred to a personal computer by a serial communications line. Figure 2 shows a vehicle with its nearside wheels on the mat. The data-logging boxes can be seen beneath the crash barrier.

Vehicle Tests

The accuracy of the mat's measurement of dynamic tire forces was assessed using a vehicle that was instrumented to measure dynamic tire forces. The vehicle was a two-axle rigid truck with single tires on the steering axle and dual tires on the drive axle. Steel spring suspensions were fitted to both axles, and the gross mass of the vehicle was 17 tons. Instrumentation fitted to the end of each axle consisted of strain gauges to measure axle bending and an accelerometer to correct for the inertia (linear and angular) of the mass outboard of the gauges (*1*). Data were logged by a digital data-logger on board the vehicle.

On-board measurements were synchronized with the mat sensor measurements by means of an infrared transmitter and detector mounted on the vehicle. The detector sensed reflective markers placed alongside the mat. Five markers were used along the length of the mat. The instrumented vehicle was driven over the mat 35 times at speeds varying from 2 m/sec to 27 m/sec (7 to 97 km/hr).

Following the instrumented vehicle tests, 14 uninstrumented articulated vehicles were tested on the mat. All the vehicles belonged to TRL and each included one of three tractor units and one of five trailers. Each vehicle was fully laden and driven over the mat about 50 times at speeds between 2 m/sec and 27 m/sec (between 7 and 97 km/hr). Table 1 describes the tractors (designated by numbers 1 to 3) and trailers (designated by letters A through E). The tractor-trailer combinations are designated by a number and a letter throughout the remainder of this paper (e.g., Vehicle 2C refers to Tractor 2 with Trailer C).

FIGURE 2 Load-measuring mat on TRL test track.

TABLE 1 Descriptions of Vehicles Tested on Load-Measuring Mat

		No. Axles	Suspension Description
Tractor 1	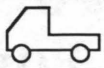	2	Steel (Multileaf) + Dampers
Tractor 2	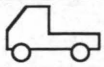	2	Air + Dampers
Tractor 3	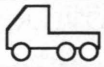	3	Steel (Multileaf)
Trailer A	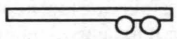	2	Wide-spread Steel Tandem (Monoleaf)
Trailer B	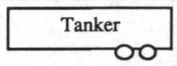	2	Wide-spread Steel Tandem (Monoleaf)
Trailer C	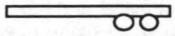	2	Rubber Tandem + Dampers
Trailer D	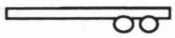	2	Air Tandem + Dampers
Trailer E	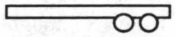	3	Steel Tri-Axle (Multileaf)

Calibration

Steering axles of articulated vehicles usually have relatively low dynamic force variation, and at low speeds the forces applied to the road surface are close to the static weights. Consequently, the mat sensors initially were calibrated using the measured static weights of the steering axles of three of the test vehicles. The static axle weights were measured by portable weigh pads.

Using this initial set of calibration factors, all of the low-speed axle force time histories measured with the mat were examined to determine which axles showed the least dynamic force variation. Five axles (two steer, one drive, and two trailer axles) were observed to have low dynamic loads. The results from a total of 23 low-speed tests for these axles were then used to determine a final set of calibration factors for the sensors in the mat.

Of the 141 sensors in the mat, three were found not to work, and seven were found to be noisy (most likely they were damaged in transit). The seven noisy sensors were included in the following accuracy calculations, but were ignored for subsequent analyses of the wheel forces.

Figure 3 shows the distribution of the root-mean-square (RMS) static error between the mat sensor measurements and the static weights (measured using weigh pads) for the final calibration runs,

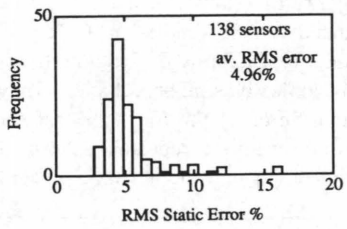

FIGURE 3 RMS error for 23 static calibration runs.

where the static error (percentage) is defined as

$$\text{static error} = 100\left(\frac{\text{static force} - \text{mat force}}{\text{mat force}}\right)\text{percent} \quad (1)$$

The average RMS error of all the sensors was 5 percent. This value can be considered the baseline accuracy of the system and compares closely with the 4 percent observed previously for a similar mat tested by Cebon and Winkler (*14*). The main difference is related to the seven noisy sensors. It is also apparent that there is a spread of sensor performance, with individual sensors showing errors as low as 2.5 percent RMS.

Instrumented Vehicle Tests

Figure 4 presents a comparison of the steering axle tire force measured by the mat and that measured on the instrumented vehicle for a speed of 25 m/sec. It is apparent from Figure 4 that the sensor measurements closely follow the on-board measurements.

Figure 5 indicates the distribution of the RMS dynamic error between all of the instrumented vehicle measurements and the mat. Here the dynamic error (in percent) is defined as

$$\text{dynamic error} = 100\left(\frac{\text{vehicle force} - \text{mat force}}{\text{mat force}}\right)\text{percent} \quad (2)$$

In this series of runs, four sensors were found not to work. Figure 5 therefore shows results from 137 sensors (including six noisy ones). The average RMS dynamic error is 6.7 percent. This error originates from several sources:

- Mat sensor error: The previous section showed that the mat sensors had an average baseline error of 5 percent RMS.
- Vehicle speed variation along the mat leading to a lack of synchronization between the markers: The relative speed variation (0.2 m/sec along the mat) was much higher at low speeds.
- Vehicle instrumentation error: An analysis of the vehicle instrumentation for straight line motion on a relatively smooth road surface suggests a contribution to the dynamic error of approximately 1.5 percent RMS (*11*). However, it is thought to be an underestimate of the source of error for the mat tests, as explained in the following.

Le Blanc et al. (*16*) examined the performance of various methods for measuring dynamic tire forces using instrumented axles. They found that the type of instrumentation system used in these measurements can generate large errors in the presence of roll or side-slip motion because of side forces and variation of the lateral position of the tire contact area. Analysis of the instrumented vehicle measurements showed that the roll component of tire force was a significant proportion of the total. Consequently, the dynamic error is likely to be greater than 1.5 percent RMS.

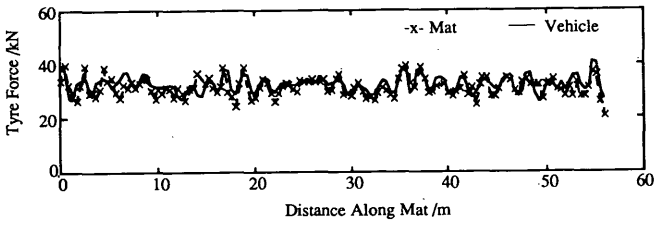

FIGURE 4 Comparison of wheel forces measured by mat and steer axle of instrumented vehicle traveling at 25 m/sec.

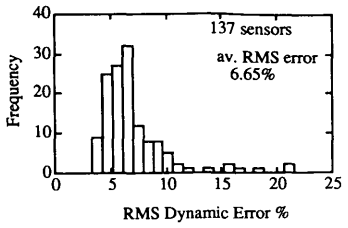

FIGURE 5 RMS error for 34 validation runs.

MEASURES OF SPATIAL REPEATABILITY

The analytical framework needed to assess the spatial repeatability of tire forces generated by heavy vehicles was presented by Cole and Cebon (*12*) and will be summarized briefly here.

Aggregate Force

The simplest measure of road loading that can be related to road damage is the "aggregate tire force" (*4,12*), which is simply the sum of the dynamic forces applied to each mat sensor by all of the axles of a vehicle. It is given mathematically by

$$A_k = \sum_{j=1}^{N_a} P_{jk} \qquad k = 1, 2, 3, \ldots, N_s \quad (3)$$

where

A_k = aggregate force at Sensor k along the mat,
P_{jk} = force applied by Tire j to Sensor k,
N_a = number of axles on the vehicle, and
N_s = number of sensors along the mat.

Aggregate force was calculated at each sensor along the mat. In order to minimize the effect of the 5 percent random sensor measurement errors, tire force histories from repeated tests of the same vehicle at the same speed were averaged together before the aggregate forces were calculated.

Aggregate Fourth-Power Force

The main disadvantage to using the aggregate force as a measure of road loading is that it does not reflect the mechanisms of road damage or the sensitivity of road materials to stress and strain levels. This disadvantage can be overcome by raising individual tire forces to a fourth power before summing their contribution at each mat sensor. This gives the aggregate fourth-power force (*12*):

$$A_k^4 = \sum_{j=1}^{N_a} P_{jk}^4 \qquad k = 1, 2, 3, \ldots, N_s \quad (4)$$

where A_k^4 is the aggregate fourth-power force at Sensor k along the mat and the exponent 4 represents the sensitivity of asphalt fatigue damage to cyclic strain level.

Spatial Repeatability Index (SRI)

To quantify spatial repeatability, aggregate tire force histories generated by each vehicle were compared with those generated by a reference vehicle. A suitable measure of spatial repeatability should indicate high repeatability when the peaks of the two force histories occur close together along the road. Low repeatability should be indicated when the peaks of one history occur near the troughs of the second history. A statistic that has this property is the correlation coefficient ρ, defined by (*17*)

$$\rho = \frac{E\{[u(t) - m_u][v(t) - m_v]\}}{\sigma_u \sigma_v} \tag{5}$$

where m_u, m_v, and σ_u, σ_v are the means and standard deviations of two signals $u(t)$ and $v(t)$, and $E\{\ \}$ is the expectation operator.

The value of ρ can be between +1 and −1. The properties of ρ may be examined by considering two sine waves of frequency ω and phase difference ϕ:

$$u(t) = \sin(\omega t) \qquad v(t) = \sin(\omega t + \phi) \tag{6}$$

In this case, Equations 5 and 6 give

$$\rho = \cos \phi \tag{7}$$

When ϕ = 0 degrees and ρ = +1, the two waves are in phase and the peaks (and troughs) of each wave occur at the same locations. When ϕ = 180 degrees and ρ = −1, the two waves are in antiphase and the peaks of one wave coincide with the troughs of the other wave.

Cole and Cebon (*12*) note that a reasonable threshold of repeatability is one-eighth of a cycle phase difference, or ϕ = 45 degrees, corresponding to a correlation coefficient of 0.707. For a speed of 22 m/sec and a frequency of 15 Hz, this threshold corresponds to a distance along the road of 0.18 m, about the length of a tire contact patch or a small pothole. For a frequency of 3 Hz, the threshold distance is 0.92 m.

SRI is defined as the correlation coefficient for an aggregate tire force history compared with a reference aggregate force history, both measured with the mat.

EXPERIMENTAL RESULTS

Effect of Speed

The effect of vehicle speed on spatial repeatability was investigated initially by calculating the SRI between the aggregate force of a reference vehicle (Vehicle 1A) traveling at a reference speed of 22 m/sec (80 km/hr) and aggregate forces for Vehicle 1A traveling at test speeds greater than and less than the reference speed. The results are presented in Figure 6, which shows that the SRI is 1.0 when the test speed is the same as the reference speed (as expected) and less than 1.0 when the test speed is different from the reference speed (22 m/sec).

Also shown in Figure 6 are the results of a simulation of the aggregate force SRI for the same Vehicle 1A from Cole and Cebon (*12*). The two results show striking similarity; however, the experimental SRI is generally less than the theoretical result by approximately 0.1, except at the reference speed. This difference is thought to be caused by the 5 percent random mat sensor error in the measurements. Note that at the reference speed, the noise is perfectly correlated with itself and therefore gives an SRI of 1.0.

Effect of Sensor Noise

Reduction in the SRI related to sensor errors may be investigated by considering the correlation between two dynamic tire forces g_1 and g_2 moving along the mat with speed V. The forces consist of sine waves of frequency ω, with added random noise:

$$g_1(x) = f_1(x) + \epsilon_1(x)$$
$$g_2(x) = f_2(x) + \epsilon_2(x) \tag{8}$$

where

$$f_1(x) = \bar{f}_1 + F_1 \sin\left(\frac{\omega x}{V}\right)$$
$$f_2(x) = \bar{f}_2 + F_2 \sin\left(\frac{\omega x}{V} + \phi\right)$$

x = distance along the mat,
$\bar{f}_1$, $\bar{f}_2$ = mean levels of $f_1(x)$ and $f_2(x)$,
F_1, F_2 = amplitudes of $f_1(x)$ and $f_2(x)$, and
ϵ_1, ϵ_2 = independent random errors with standard deviations σ_{ϵ_1} and σ_{ϵ_2}.

From Equations 5 and 8, the SRI for the modified sine waves becomes

$$SRI = \frac{\dfrac{\omega}{2\pi V}\displaystyle\int_0^{2\pi V/\omega} [g_1(x) - \bar{f}_1][g_2(x) - \bar{f}_2]dx}{\sigma_{g_1}\sigma_{g_2}} \tag{9}$$

In general, ϵ_1 and ϵ_2 are different functions of distance (although they are likely to have the same statistics), and they are both

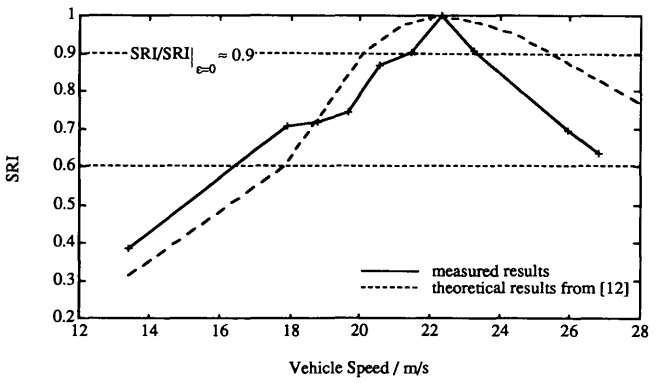

FIGURE 6 Measured and predicted SRI values for Vehicle 1A.

uncorrelated with $\sin(\omega x/V)$. Equation 9 then reduces to

$$SRI = \frac{\sigma_{f_1}\sigma_{f_2}\cos\phi}{\sqrt{(\sigma_{f_1}^2 + \sigma_{\epsilon_1}^2)(\sigma_{f_2}^2 + \sigma_{\epsilon_2}^2)}} \quad (10)$$

where σ_{f_1} and σ_{f_2} are the RMS values of $f_1(x)$ and $f_2(x)$.

Now consider the value of the SRI for two tests of the same vehicle at speeds near the reference speed (i.e., near 22 m/sec in Figure 6). Assuming the RMS dynamic loads for the two runs are approximately equal, $\sigma_{f_1} \approx \sigma_{f_2} = \sigma_f$, and that the amount of noise on the two measurements is similar, $\sigma_{\epsilon_1} \approx \sigma_{\epsilon_2} = \sigma_\epsilon$, Equation 10 can be rewritten as

$$\frac{SRI}{SRI|_{\epsilon=0}} = \frac{1}{[1 + (\sigma_\epsilon/\sigma_f)^2]} \quad (11)$$

where $SRI|_{\epsilon=0}$ is the SRI for the signals with no noise (from Equation 10) and σ_ϵ/σ_f is the ratio of RMS noise to RMS dynamic wheel load.

It can be seen from Equation 11 that for a given dynamic tire force level (σ_f), increasing the noise level decreases the maximum possible correlation between the two signals. If there is no noise ($\sigma_\epsilon/\sigma_f = 0$), the maximum possible SRI is 1.0. However, if the RMS noise level is equal to the RMS of the dynamic load (i.e., $\sigma_\epsilon/\sigma_f = 1$), the maximum possible SRI for the two signals is 0.5. Note that if a noisy signal is correlated with itself, $\epsilon_1(x) = \epsilon_2(x)$, and the SRI will be 1.0, irrespective of the fact that the signal contains some noise.

In order to estimate the maximum possible SRI from Equation 11, the standard deviations of the dynamic load and noise are both required. The standard deviation of the sensor error previously was found to be 5 percent of the average static load. The standard deviation of three averaged measurements (from the three test runs at 22 m/sec) is therefore $\sigma_\epsilon = 5/\sqrt{3} = 2.9$ percent. Knowing the standard deviation of the dynamic load plus noise (measured with the mat) and the standard deviation of the noise alone, it is possible to calculate the standard deviation of the dynamic load alone, σ_f for each axle. For the drive axle of Vehicle 1A, σ_f is approximately 8.7 percent of the static load. Substituting these values into Equation 11 gives a maximum possible SRI of approximately 0.9.

If the aggregate force history is used, as opposed to a single force history, this value of 0.9 can be shown to be a lower bound; the true value will be slightly higher. The value of 0.9 is marked on Figure 6 and can be seen to be a reasonable lower-bound estimate of the maximum SRI at the reference speed.

Because of the reduction in SRI related to noise, the threshold value of SRI in this study is 0.6 instead of 0.7 (see previous section). Figure 6 shows that the SRI is above this threshold value for speeds approximately 6 m/sec, on either side of the reference speed.

Effects of Vehicle Configuration

Figure 7 shows results for Vehicles 1A, 1B, 1C, 1D, and 1E at various speeds, correlated with the reference vehicle (Vehicle 1A) traveling at the reference speed of 22 m/sec. These vehicles all have the same tractor, with six different trailers (see Table 1). All the vehicles show a peak in SRI near the reference speed. The maximum SRI values range from 0.85 for Vehicle 1C to 0.58 for Vehicle 1D.

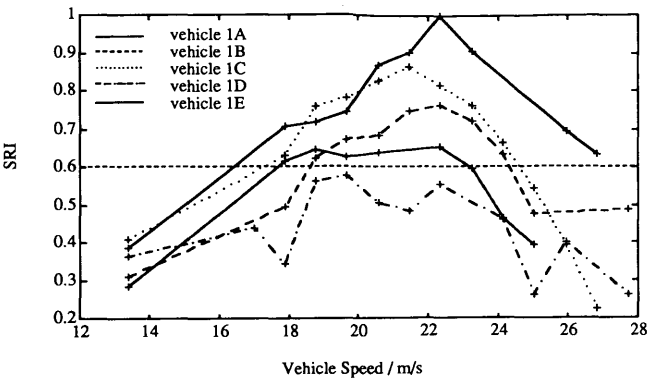

FIGURE 7 SRI for Vehicles 1A, 1B, 1C, 1D, and 1E; Vehicle 1A is reference vehicle.

In their theoretical study, Cole and Cebon [*12*] considered the dominant wavelength of the aggregate force history to be the main factor in determining the correlation between vehicles. (The dominant wavelength was calculated by dividing the speed by the dominant frequency component in the aggregate force spectral density.) Vehicle 1D includes a steel-sprung tractor and an air-sprung trailer. It is likely that the aggregate force history of this vehicle is not dominated by a single wavelength (*12*), and therefore the correlation with the reference vehicle is low. All the other vehicles (steel-sprung trailers and a rubber-sprung trailer) have trailer suspensions with similar stiffnesses to that of the reference vehicle and are likely to have similar dominant wavelengths. They therefore have maximum SRIs above the threshold of 0.6.

Figure 8 shows the corresponding graph for Vehicles 2A, 2B, 2C, 2D, and 2E, using Vehicle 2A at 22 m/sec as the reference (see Table 1). The SRIs vary less with speed than for Vehicles 1A through 1E (Figure 7). The reason for this is not yet known but may relate to the combination of dissimilar suspensions on the tractor and trailer, leading to the absence of a single dominant wavelength in the aggregate forces.

Figure 9 shows the results for Vehicles 3A, 3B, 3D, and 3E, using Vehicle 3A at 22 m/sec as the reference (see Table 1). All the vehicle combinations presented in Figure 9 (apart from the reference) display low repeatability. The tractor used in all these

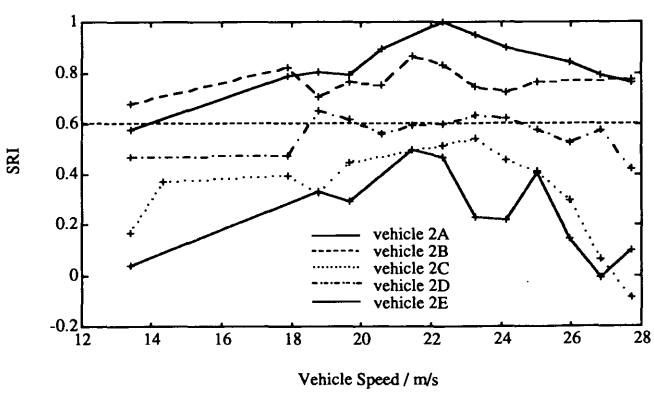

FIGURE 8 SRI for Vehicles 2A, 2B, 2C, 2D, and 2E; Vehicle 2A is reference vehicle.

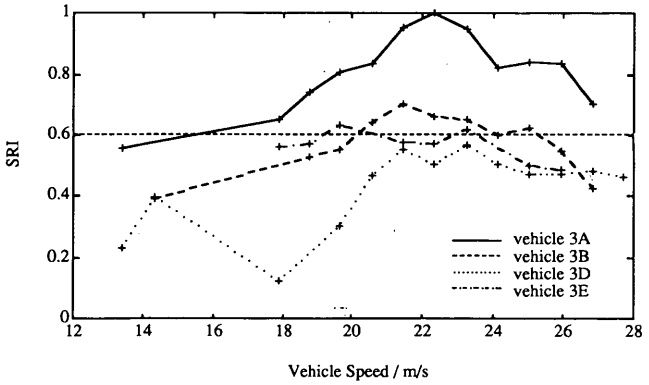

FIGURE 9 SRI for Vehicles 3A, 3B, 3D, and 3E; Vehicle 3A is reference vehicle.

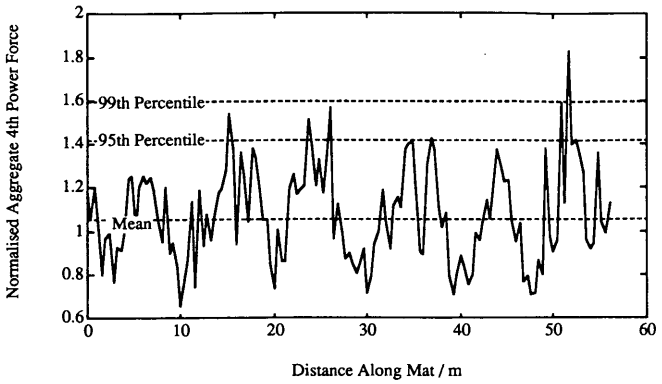

FIGURE 11 Normalized aggregate fourth-power forces for 140 vehicle runs.

vehicle combinations (Tractor 3) had a stiff tandem drive axle suspension with lightly damped axle pitch and body bounce modes of vibration. Possible causes of the low repeatability are (*a*) poor correlation because of the high-frequency tandem pitching mode, and (*b*) an increase in sensitivity to changes in the trailer suspension group caused by the stiff tractor suspension. These causes are the subject of current investigations.

Figure 10 indicates SRIs for the 14 vehicles traveling at 18 m/sec correlated with Vehicle 1A also traveling at 18 m/sec. The vehicles are ordered along the horizontal axis in descending order of correlation at this speed. The graph also shows the corresponding results for the speeds of 22 and 26 m/sec. In these cases the reference vehicle is Vehicle 1A, traveling at 22 and 26 m/sec, respectively.

For all three speeds, the SRI decreases as the vehicle becomes less similar to the reference vehicle. Most of the vehicles with the reference tractor (Tractor 1) have relatively high SRIs, and the vehicles most different from the reference vehicle tend to have low SRIs. This is particularly evident for Tractor 3, with its stiff tandem leaf-spring suspension, and Trailer D, which has an air suspension. Approximately half of the data points in Figure 10 have SRIs above 0.6, indicating that approximately half of the vehicles in this general class are likely to contribute to a repeatable pattern of road loading. However, it should be noted that the vehicles tested were of very diverse configurations and not representative of the highway fleet.

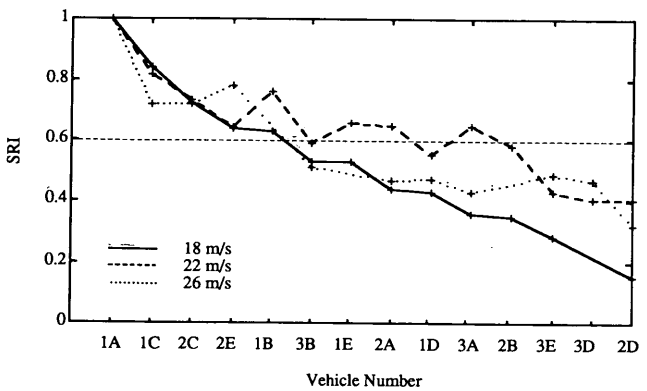

FIGURE 10 Ordered SRI for all vehicles for different reference speeds.

Aggregate Fourth-Power Force

Figure 11 shows the accumulated damage caused by 140 aggregate fourth-power force histories (Equation 4) for the 14 different vehicles. The results have been normalized by the damage from the static tire forces alone (i.e., a value of 1 corresponds to the damage caused by the static axle loads of the 140 vehicle passes). Despite the wide range of vehicles and speeds used in this study, there is a dominant wavelength of approximately 8 m in the aggregate fourth-power force history. This wavelength probably is associated with the sprung mass modes of vibration of the vehicles. It agrees reasonably well with the 7 m predicted by Cole and Cebon (*12*). The peak damage is approximately 1.8 times that caused by the static loads alone.

The horizontal lines on Figure 11 show upper-percentile levels of A_k^4. The 95th-percentile level of damage is 1.4 times the static damage (from the static loads alone). If it was assumed that there was no spatial repeatability (dynamic forces randomly distributed along the road), the damage would be uniformly distributed along the road at the mean level, which is 1.05 times the static damage. Spatial repeatability therefore causes a significant increase in the damage caused at some locations along the road surface by dynamic loads, even for the relatively smooth surface of the TRL test track.

CONCLUSIONS

1. The wheel load measuring mat is sufficiently accurate for measuring the dynamic tire forces of heavy vehicles. The sensors have an average baseline accuracy of 5 percent RMS, which compares closely with the 4 percent measured in a previous study. Some sensors were found to have much better performance than average, with baseline errors as low as 2.5 percent RMS.
2. The correlation between the aggregate force distributions generated by different vehicles depends strongly on the speed as well as the combination of tractor-trailer suspensions.
3. Approximately half of the articulated vehicles tested were found to contribute to a spatially repeatable pattern of road loading.

4. For a fleet of vehicles consisting of all the vehicles tested in the study, the fatigue damage incurred by 5 percent of the road surface would be approximately 1.4 times the fatigue damage from the static loads alone. This value would be expected to increase significantly for rougher roads.

5. The experimental results of this study largely confirm earlier theoretical predictions.

6. The implication of conclusions (3) and (4) is that fatigue failure of roads is likely to be governed by peak dynamic forces. Consequently, any measure of vehicle dynamic loading performance should consider these peak forces rather than average dynamic forces.

ACKNOWLEDGMENTS

The authors are very grateful to the Science and Engineering Research Council for funding the research described in this paper; to the director of the Transport Research Laboratory and members of the Vehicle and Environment Division for providing the test track, vehicles, and technical support and for installing the mat; and to Golden River Traffic Ltd., and the University of Michigan Transportation Research Institute for their assistance with the provision of the load-measuring mat.

REFERENCES

1. Mitchell, C. G. B. and L. Gyenes. Dynamic Pavement Loads Measured for a Variety of Truck Suspensions. *Proc., 2nd International Conference on Heavy Vehicle Weights and Dimensions*, Kelowna, British Columbia, Canada, 1989.
2. Monismith, C. L., J. Sousa, and J. Lysmer. Modern Pavement Design Technology Including Dynamic Load Conditions. *Proc., SAE Conference on Vehicle/Pavement Interaction*, SP765, Society of Automotive Engineers, Warrendale, Pa., 1988.
3. O'Connell, S., E. Abbo, and K. Hedrick. Analyses of Moving Dynamic Loads on Highway Pavements; Part I. Vehicle Response. *Proc., International Symposium on Heavy Vehicle Weights and Dimensions*, Kelowna, British Columbia, Canada, 1986.
4. Cebon, D. *An Investigation of the Dynamic Interaction Between Wheeled Vehicles and Road Surfaces*. Ph.D. thesis. University of Cambridge, Cambridge, England, 1985.
5. Ervin, R. D., et al. *Influence of Truck Size and Weight Variables on the Stability and Control Properties of Heavy Trucks*. Transportation Research Institute, University of Michigan, Ann Arbor, 1983.
6. Hahn, W. D., *Effects of Commercial Vehicle Design on Road Stress: Vehicle Research Results*. Institut für Kruftfahrwesen, Universität Hannover, Germany, 1985.
7. Addis, R. R., A. R. Halliday, and C. G. B. Mitchell. Dynamic Loading of Road Pavements by Heavy Goods Vehicles. *Proc., Congress on Engineering Design, Seminar 4A-03*, Institution of Mechanical Engineers, Birmingham, England, 1986.
8. Woodrooffe, J. H. F., P. A. LeBlanc, and A. T. Papagiannakis. Suspension Dynamics: Experimental Findings and Regulatory Implications. *Proc., SAE Conference on Vehicle and Pavement Interaction*, SP765, Society of Automotive Engineers, Warrendale, Pa., 1988.
9. Gyenes, L. and C. G. B. Mitchell. The Spatial Repeatability of Dynamic Pavement Loads Caused by Heavy Goods Vehicles. *Proc., Third International Symposium on Heavy Vehicle Weights and Dimensions*, Cambridge, England, Thomas Telford, London, England, 1992.
10. Cebon, D. Vehicle-generated road damage: A Review. *Vehicle System Dynamics*, Vol. 18 (1–3), 1989, pp. 107–150.
11. Cole, D. J. *Measurement and Analysis of Dynamic Tyre Forces Generated by Lorries*. Ph.D. thesis. Cambridge University, Cambridge, England, 1990.
12. Cole, D. J. and D. Cebon. Spatial Repeatability of Dynamic Tyre Forces Generated by Heavy Vehicles. *Proceedings of the Institution of Mechanical Engineers, Part I. Journal of Automobile Engineering*, Vol. 206, 1992, pp. 17–27.
13. Cole, D. J. and D. Cebon. A Capacitative Strip Sensor for Measuring Dynamic Tyre Forces. *Proc., 2nd Int. Conf. on Road Traffic Monitoring*, Institute of Electrical Engineers, London, England, 1989.
14. Cebon, D. and C. B. Winkler. *A Study of Road Damage Due to Dynamic Wheel Loads Using a Load Measuring Mat*. Strategic Highway Research Program, Final Report, UMTRI-90-13, Vol. 1, National Research Council, Washington, D.C., 1990.
15. Cebon, D. and C. B. Winkler. Multiple-Sensor Weigh-In-Motion: Theory and Experiments. In *Transportation Research Record 1311*, TRB, National Research Council, Washington, D.C., 1991, pp. 70–78.
16. Le Blanc, P. A., J. H. Woodrooffe, and A. T. Papagiannakis. A Comparison of Two Types of Instrumentation for Measuring Vertical Wheel Load. *Proc., Third International Symposium on Heavy Vehicle Weights and Dimensions*, Cambridge, England, Thomas Telford, London, England, 1992.
17. Newland, D. E. *Random Vibrations and Spectral Analysis*, 2nd edition. Longman, 1985.

Publication of this paper sponsored by Committee on Strength and Deformation Characteristics of Pavement Sections.